Computers and Electronics in Agriculture 202 (2022) 107414

Contents lists available at ScienceDirect

Computers and Electronics in Agriculture

journal homepage: www.elsevier.com/locate/compag

A novel heat-pulse probe for measuring soil thermal conductivity: Field test under different tillage practices

Ahmed Abed Gatea Al-Shammary [a,**], Andrés Caballero-Calvo [b,*], Hussein Abbas Jebur [c], Mohanad Ismael Khalbas [a], Jesús Fernández-Gálvez [b]

[a] Soil Science and Water Resources Departments, College of Agriculture, University of Wasit, Kut, Iraq
[b] Department of Regional Geographical Analysis and Physical Geography, University of Granada, 18071 Granada, Spain
[c] Department of Agricultural Machines and Equipment, College of Agricultural Engineering Sciences. University of Baghdad, Iraq

ARTICLE INFO

Keywords:
Soil thermal conductivity
Heat-pulse-probe design
Soil management practices
Tillage practices
Fertilizer treatments

ABSTRACT

Accurate soil thermal conductivity (λ) measurements are needed in experimental agri-environmental research. This study design and build of new heat-pulse probe (HPP) based on transient state technology to measure λ. The HPP consists of three main components: an electronic control system, a measurement chamber, and sample rings. The performance of the new HPP for in-situ λ measurements is compared to estimates from measurable soil physical properties (pedotransfer function). Tests were conducted in clay loam and loam soils at three depths. λ measurements by the HPP were affected by tillage practice, fertilizer treatment, soil depth, and soil type. No significant differences in λ measurements by the HPP and estimates from a pedotransfer function were found between tillage practices. There were positive correlations between their values at three soil depths: $R^2 = 0.92$ at 0–5 cm depth, and $R^2 = 0.88$ at both 5–10 and 10–15 cm depths. The standard deviation from the HPP measurements were 0.061, 0.077, and 0.080 $W{\cdot}m^{-1}{\cdot}K^{-1}$ at 0–5, 5–10, and 10–15 cm depths, respectively. In contrast, the pedotransfer function estimates had standard deviations of 0.085, 0.660, and 0.083 $W{\cdot}m^{-1}{\cdot}K^{-1}$, respectively. It was found that conventional tillage increases temperature flow in soils compared to no-tillage because of decreasing soil bulk density (ρb) and consequently higher porosity. The proposed HPP is a low-cost and energy-efficient device, with wide applicability under a range of conditions. It is highly recommended for measuring λ clay loam and loam soils; however, more research is needed to determine its value with other soil types.

1. Introduction

Soil thermal conductivity (λ) is a key thermal property used in a range of energy calculations in geotechnical and agri-environmental applications (Kojima et al., 2021; Zhao et al., 2019) as well as the most important property in studying soil thermal conditions (Tarnawski et al., 2020). It influences the soil thermal regime and can be used as an indicator of soil processes, such as microbial organic content (Taghizadeh-Toosi et al., 2019), air-filled porosity (Usowicz et al., 2006), soil bulk density (Mahdavi et al., 2016), soil water content (Romio et al., 2019), soil texture (Nikoosokhan et al., 2016), soil temperature (Morris et al., 2010), soil structure, and soil mineralogy (Schjønning, 2021).

Soil λ can be defined as the ability of the soil to transfer heat through a unit thickness under a unit temperature difference (Chen et al., 2020; Schjønning, 2021). It is more precisely linked with the transfer of heat across soil by radiation, conduction, and convection (Muhammad et al., 2018). Soil λ can also be used as an indicator of the thermal flux density of soil (Romio et al., 2019).

There are two types of methods for measuring λ depending on how the variation of temperature (ΔT) is considered with time (t): steady-state (SS; $\partial T/\partial t = 0$, or transient-state (TS; $\partial T/\partial \tau \neq 0$) (Bristow, 1998; Zhaoxiang and Jingsen, 1983). SS methods determine λ by measuring ΔT at a constant distance through a constant heat flow across a soil sample, then estimating λ directly using Fourier's Law (Zhao et al., 2019). There are four types of SS techniques: the absolute technique (AT), the comparative technique (CT), the radial heat flow technique

* Corresponding author.
** Corresponding author.
E-mail addresses: agatea@uowasit.edu.iq (A. Abed Gatea Al-Shammary), andrescaballero@ugr.es (A. Caballero-Calvo), dr.hussain@coagr.Uobaghdad.edu.iq, hussainjebur@gmail.com (H.A. Jebur), albwmohanad@uowasit.edu.iq (M. Ismael Khalbas), jesusfg@ugr.es (J. Fernández-Gálvez).

https://doi.org/10.1016/j.compag.2022.107414
Received 8 May 2022; Received in revised form 2 August 2022; Accepted 25 September 2022
Available online 4 October 2022

(RHFT), and the parallel thermal conductance technique (PTCT). The main drawbacks of the SS methods are the required thermal insulation to reduce edge or end effects (He et al., 2018b) as well as the long time needed to achieve heat balance. To overcome these limitations, TS methods were developed (He et al., 2020a) based on the dissipation of energy as a function of time, where λ is estimated by the energy conservation law. There are also four types of TS techniques: flow heat pulse (FHP), hot wire (HW), transient plane source (TPS), and the laser flash technique for thermal diffusivity (LFTTD). The main advantages of the TS methods are reasonable measurement time and cost, as well as suitability for field application (Dong et al., 2014; Maivald et al., 2022).

The FHP is the most widely used technique for measuring soil thermal properties, such as λ, and has a long history (He et al., 2020b; Liu et al., 2020; Wang et al., 2020). The two main types of FHP methods include single-probe heat-pulse (SPHP) and dual-probe heat-pulse (DPHP), either using a single or dual heat-pulse probe, respectively (He et al., 2020a; Wang et al., 2021).

Most of these methods have accuracy limits based on the temperature range and soil properties, as λ is influenced especially by soil water content (Du et al., 2022), soil texture (Różański, 2022), and soil temperature regime (He et al., 2022; Lu et al., 2020). These variables have a significant influence on crop growth and yield and other soil ecosystem services. Numerous studies have improved FHP methods for measuring λ (He et al., 2018a; Wang et al., 2020; Zhang et al., 2014) by identifying the causes of inaccuracy and conducting tests on soils with different textures (Knight et al., 2012).

Due to technical difficulties (specific training and electricity), cost, and intrinsic variability ((He et al., 2020a); estimates of λ commonly come from more easily available soil information by using pedotransfer functions (Al-Maliky, 2011; Jameel Kareem Al-Lame and NA Al-

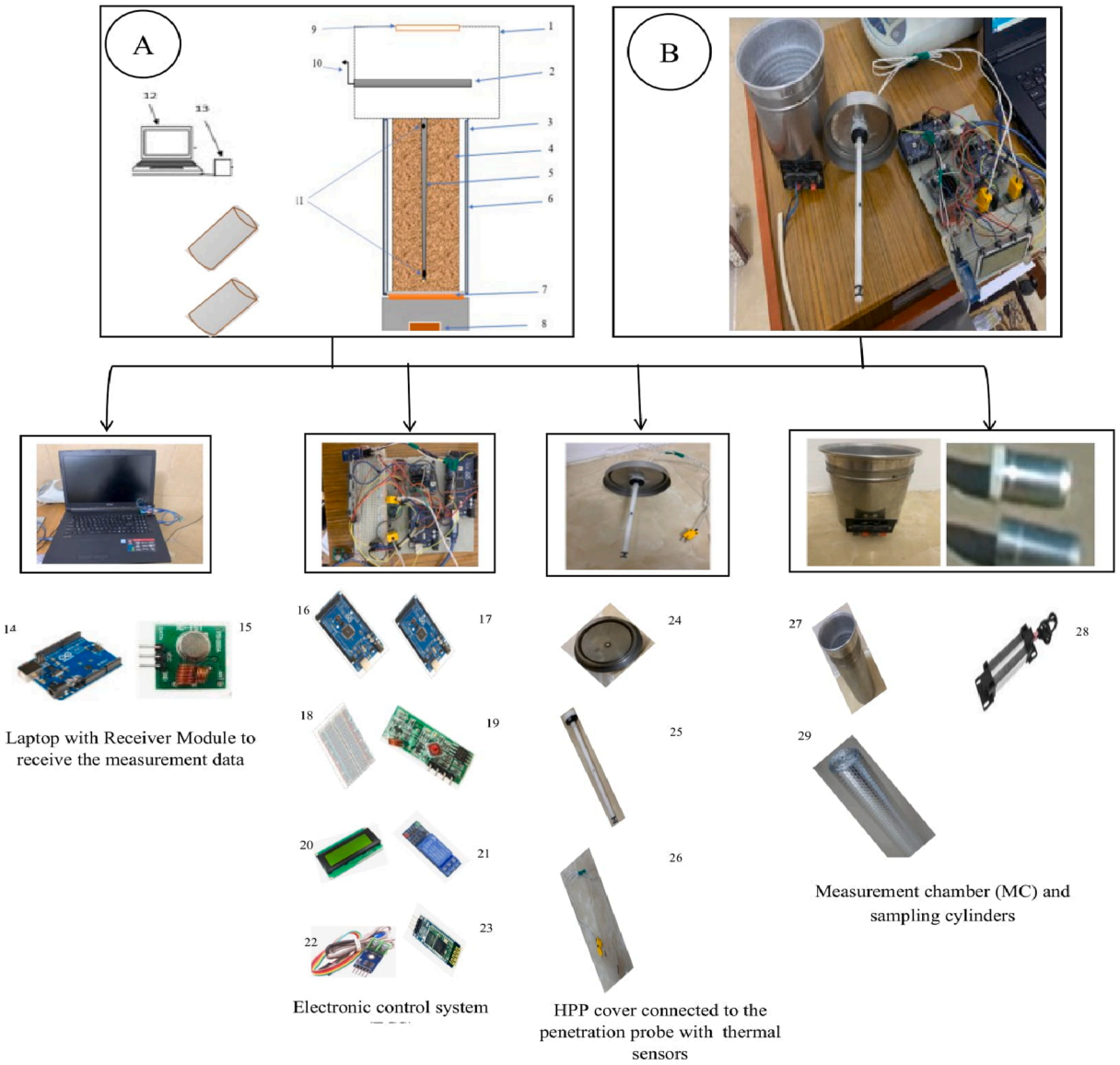

Fig. 1. A: Diagrams and B: photograph of the new heat-pulse-probe designed for measuring soil thermal conductivity. Fig. 1A presents the following parts; 1) electronic control system; 2) electronic circuits; 3) measurement chamber; 4) soil sample; 5) penetration probe; 6) cylindrical plate with thermal insulation; 7) electric heater; 8) power socket; 9) LCD screen; 10) antenna for RF transmitter module; 11) two thermocouples type K; 12) laptop; 13) microcontroller with receiver module to receive measurement data. Fig. 1B showed the following parts:14) Arduino board used to receive measurement data and transfer to laptop; 15) 315 MHz RF receiver module; 16) Arduino ATmega2560 recorded soil temperatures of soil sample with time; 17) Arduino ATmega2560 responsible for providing a power source and controlling the electric heater; 18) Breadboard; 19) RF transmitter module; 20) LCD display; 21) current sensor (Acs 712);22) MAX6675 thermocouple amplified; 23) Bluetooth module HC-05; 24) stainless-steel cover; 25) stainless-steel probe penetration; 26) two thermocouples type K; 27) cylindrical measurement chamber; 28) electric heater (12 V); 29) thermal insulation of measurement chamber.

Saadoon, 2020). Therefore, there is a need for an accurate HPP combining low cost and energy efficiency.

Natural conditions (soil texture, lithology, depth) and land management (tillage, mulching, and fertilizers) affect soil compaction and water holding capacity (Mirzaei et al., 2022). They change the spatio-temporal characteristics of both bulk density (ρ_b) and volumetric soil water content (θ) (Walczak and Usowicz, 1994), leading to changes in λ that influence vegetation development (Sandholt et al., 2002; Zhou et al., 2007).

This study designed a novel HPP based on the TS technique consisting of an electronic control system and a measurement chamber. The device is more accurate, cheap, and energy-efficient than existing FHP systems. It can be built using commonly available components and tools. Furthermore, the new HPP is tested for measuring λ at three depths in two soil types (clay loam and loam) located in the middle and southern parts or Iraq under different soil management practices (tillage and fertilizers). Measurements of λ with the new HPP are also compared to estimates using the pedotransfer function from Evett et al. (2012).

2. Materials and methods

2.1. Heat-pulse probe design and implementation

A schematic diagram of the HPP presented in this work is shown Fig. 1. It is designed and built based on the TS method with a cylinder-shaped body so that the design can measure the thermal conductivity and electro-thermal coefficient. The TS method is derived from the absolute technique of the SS method but with the difference that it uses a periodic electric heating current, I(t). Also, the heat interval used for the HP techniques is considerably shorter than that used in SS methods (Shiozawa and Campbell, 1990), therefore redistribution of soil water during measurements is minimal.

The HPP uses using commercially available materials and does not require high-level skills to be built, making it inexpensive and easy to maintain and operate. Heat is transferred through the soil by a constant heat source, and ΔT is measured over a constant distance in the soil by temperature sensors. The equipment used in the new HPP consists of several units: an electronic control system, HPP cover, a measurement chamber, wireless communication, and sample rings (Fig. 1).

2.1.1. Electronic control system (ECS)

The ECS is responsible for the control and data analysis of λ measurements. The main purpose of the ECS is to control the temperature of the electric heater, measure the soil sample temperature, and record data on a PC. As shown in Fig. 1B it consists of:

A. Liquid crystal display (LCD 12C; 16 columns and 2 rows) showing the soil temperatures measured by thermocouples and the soil thermal conductivity value.
B. Arduino board (Two Arduino ATmega2560-16AU Board, China): Two Arduino Mega 2560 board has been chosen, one board used the thermocouples with MAX6675 module for measuring soil temperature, also coupled with RF Transmitter Module for transferring data to a PC. The second board is used for controlling and connecting to the electric heater, with bluetooth module as a receiver in wireless communication.
C. HPP cover, stainless-steel, diameter = 10 cm. It is serrated on the inside to facilitate connection to the measurement chamber (MC). The cover is connected to the penetration probe with thermal sensors (Fig. 1B).
D. Penetration probe, consisting of a stainless-steel probe, 15 cm in length, with a pointed end. Its function is to insert the thermocouples into the soil sample.
E. Thermocouples: Two thermocouples type K are located along with the penetration probe, as shown in Fig. 1B. To maintain the dynamic range of the analog-to-digital converter of the Arduino board, the measured voltage from the thermocouple is amplified by two MAX6675 thermocouple operations (Fig. 2A).
F. 315 MHz RF Transmitter and Receiver Modul:The RF Transmitter module is used to transfer the measurement data from Arduino-ATmega2560 to a PC by wireless communication. It uses the Arduino-microcontroller with a receiver module to receive the measurement data and finally data is recorded in a PC (Fig. 2A,B).
G. Current sensor (Acs 712): A sensor that detects electric current entering the heater. It is connected with the heater in series (Fig. 1B and 3).
H. A 5 V relay to control a high-current using a low-current signal designated to interface with the Arduino board and a switch with a fused connection to connect and disconnect the power supply (Fig. 3).
I. Bluetooth module HC-05: The HC-05 module is used to control operation of the electric heater (Fig. 3).
J. Power supply, either from a socket or a generator.

2.1.2. Measurement chamber

The measurement chamber (MC) has a cylindrical body of 1 cm thick, 8 cm in diameter, and 10 cm in height, made of stainless steel and serrated on the external upper side. The MC contains:

A. Thermal insulation: The sides are filled with a 2 mm thickness aluminiumm bubble foil thermal insulation with thermal conductivity lower than 0.03 $W{\cdot}m^{-1}{\cdot}K^{-1}$ to reduce heat loss from the MC.
B. Cylindrical plate: An steel plate of 0.1 cm thick, that surrounds the thermal insulation material to fix it in place.
C. Electric heater (12 V): A heat source with 100 W power wraps the heater and is fixed by brackets on the aluminium plate.
D. Insulation pipe: Used to protect the electric cables that transfer power from the ECS unit to the electric heater.

2.1.3. Sampling cylinders

Cylinders are made of stainless steel with a diameter of 6 cm and a height of 9 cm. They allow undisturbed soil samples to be transferred from the field to the HPP while retaining the soil's natural characteristics.

2.2. Measuring λ using the novel HPP

The new HPP is designed to measure λ according to the following procedure implemented in the firmware, which is represented by the flow chart in Fig. 4.

First, undisturbed soil samples are collected in their natural state; i.e., preserving soil porosity and structure. Cylinders made of stainless steel were designed for this purpose. Samples are taken by pushing the cylinder into the soil to the required depth (vertical or horizontally according to the requirements) using a flat piece of wood that is larger than the cylinder diameter. The wood may be hammered if the soil is dry or pushed by hand if it is wet. Then, the cylinder is drawn out and covered at the top and bottom with rubber seals. The sample is inserted carefully into the MC of the HPP to ensure that the soil structure is not disturbed.

After inserting the soil sample into the MC of the HPP, the removable ECS is attached tightly to the MC before the power is turned on using the HPP switch. The soil temperature is recorded before applying heat using the thermocouple sensors (<15 s). The digital output signal of the Arduino board is connected to the electric heater (on), which is controlled by a relay. Because it is not possible to control or connect this relay directly to the Arduino board, it is necessary to connect a 1-channel 5-V relay module to record the heat power over time.

The electrical power consumed by the heater per unit time is calculated using the Arduino board, which measures the incoming voltage and current and the resistance of the heater. During the sample heating stage until time = 1 min, the Arduino board reads the thermocouple to determine the sample temperature overtime at two points

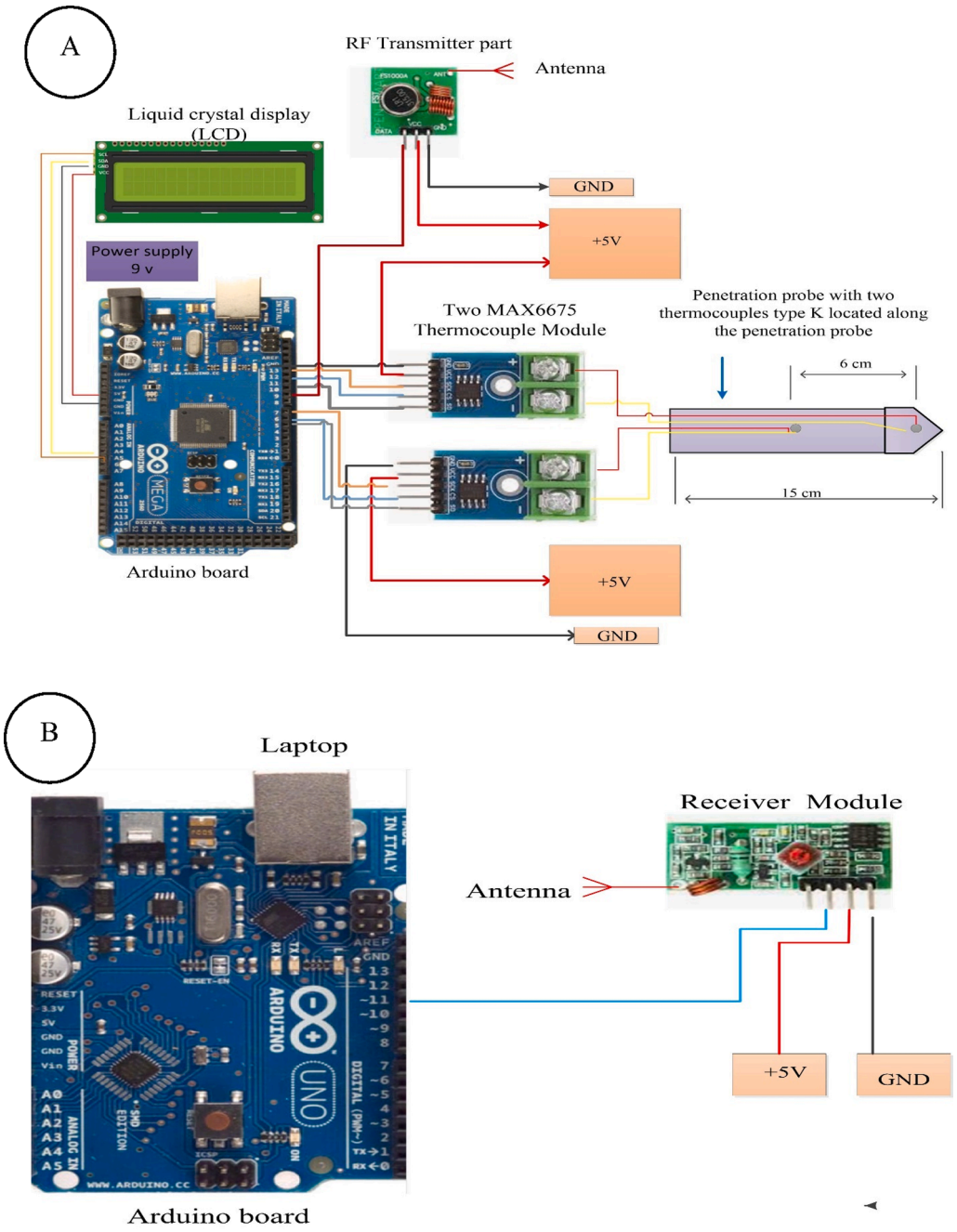

Fig. 2. A: Diagram of thermocouples with MAX6675 module, RF transmitter module circuit, Fig. 2B shows the circuit for the receiver module used in the HPP.

using the penetration probe. The Arduino board calculates the temperature difference (ΔT) at the two locations of the soil with time.

To calculate the soil thermal conductivity, the data recorded previously are entered into software. The results of λ with measured time are sent to the LCD screen for display. Outputs were analysed using SAS 9.4v.

2.3. HPP testing and study sites description

The HPP was tested by measuring λ two sites at three depths under different land management in the middle and southern parts of Iraq. A total of 18 soil treatments were identified at each site in three soil layers. The two experimental sites were the Al Qataniyah village experiment (QVE) and the Al-Zafaraniah farm experiment (ZFE). Random soil samples were taken horizontally at depths of 0–5 cm, 5–10 cm, and 10–15 cm to assess the physicochemical characteristics (Sparks et al., 2020). Sampling was conducted before tillage operations, as shown in Table 1. The QVE is located near Aziziyah city, Wasit, Iraq (32.91° N, 44.9° W), and measurements were taken in October 2021 on a site with a clay loam soil (Soil Survey Staff, 2014) (21 % sand, 40 % silt, 39 % clay at 0–5 cm soil depth; 23 % sand, 44 % silt, 33 % clay at 5–10 cm; and 26 % sand, 40 % silt, 34 % clay at 10–15 cm). The soil was abandoned in 2014, but it was planted with different species of crops such as wheat, maize, alfalfa, and rice before 2014. Current natural vegetation was schanginia aegyptiaca. The last tillage was down to 15 cm depth with a mouldboard plough. Since then, the soil has not been subject to ploughing or traffic. The soil surface was stable and undisturbed. The ZFE is located in Baghdad, Iraq (33.26° N, 44.46° W). At this site, measurements were taken in September 2021 in a loam soil (Soil Survey Staff, 2014) (38.2 % sand, 42.7 % silt, 19.1 % clay at 0–5 cm soil depth;

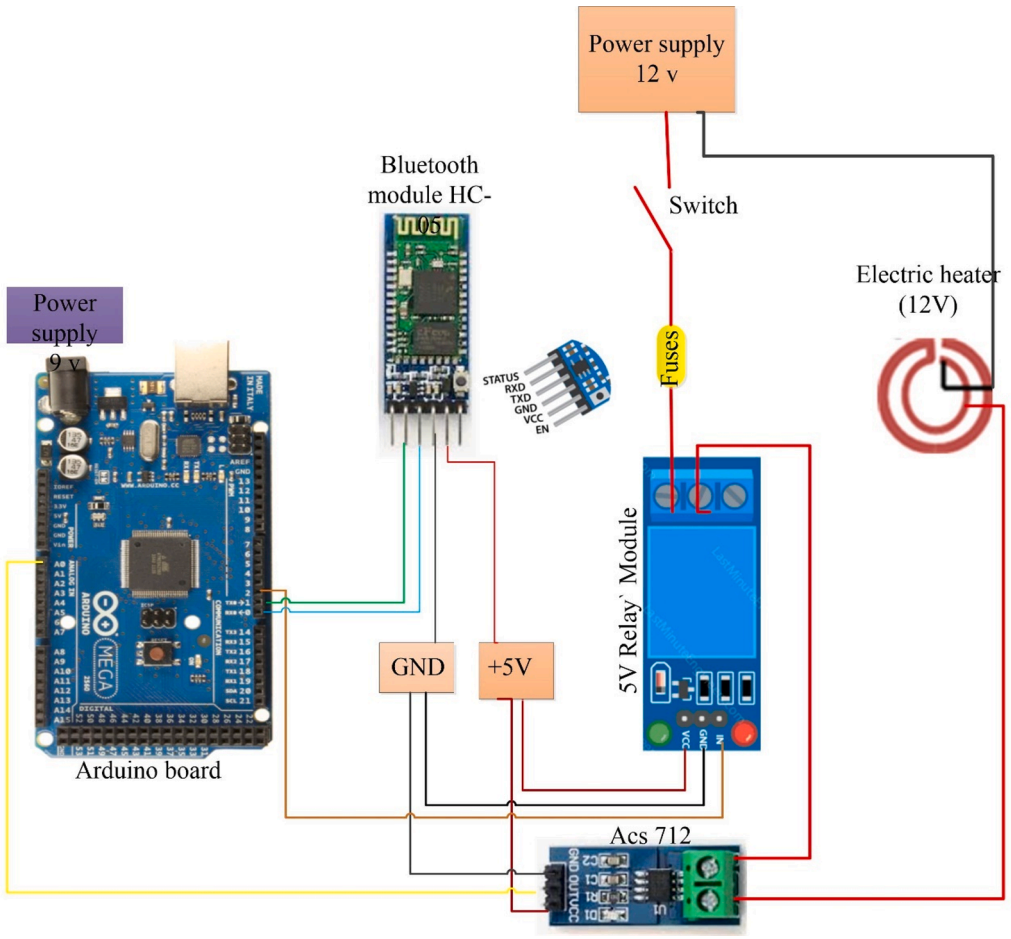

Fig. 3. Circuit diagram of the electric heater control and electrical load detection, coupled with the HC-05 Bluetooth module.

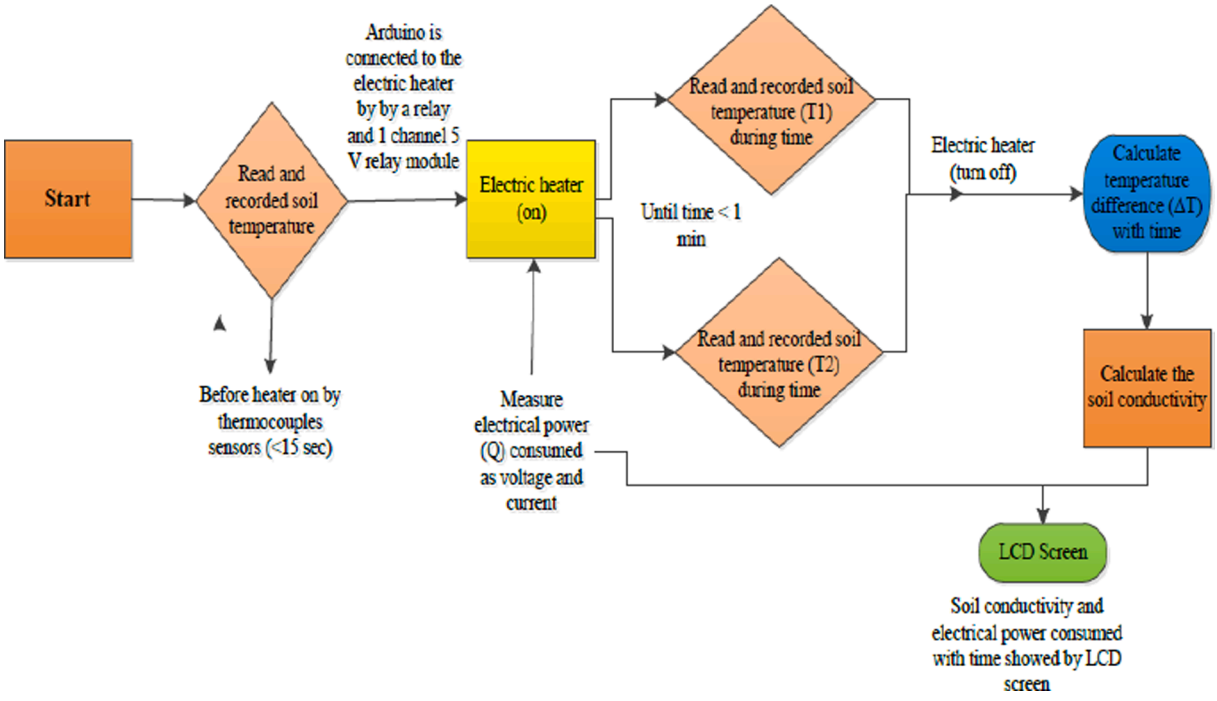

Fig. 4. Algorithm used by the firmware of the proposed heat-pulse probe to measure soil thermal conductivity.

Table 1
Soil characteristics of the two experimental sites.

Sites ID	Soil depth (cm)	Volumetric soil water content (θ; %)	Soil organic matter (SOM; %)	Soil dry bulk density (ρ_b; g cm^{-3})	pH	EC Ds m^{-1}	Particle size distribution (%)			Texture
							Clay	**Silt**	**Sand**	
QVE	0–5	20.7	7.6	1.33	7.14	1.79	39	40	21	Clay loam
	5–10	24.2	8.0	1.36	7.10	1.70	33	44	23	
	10–15	28.6	7.6	1.42	7.07	1.66	34	40	26	
ZFE	0–5	18.0	7.1	1.43	7.10	1.76	19	43	38	loam
	5–10	25.0	7.0	1.48	7.07	1.70	20	34	46	
	10–15	27.0	7.1	1.51	7.00	1.62	13	37	50	

46 % sand, 34 % silt, 20 % clay at 5–10 cm; and 50 % sand, 37 % silt, 13 % clay at 10–15 cm). The crop monitored at this experiment site was wheat, which is the most extensively used crop in this region.

The soil texture at the experimental sites was determined using the sieve-hydrometer method (Huluka and Miller, 2014). The bulk density (ρ_b) and soil water content (θ) were measured by core sampling followed by weight and oven-dried weight (ASTM, 2010). ρ_b was calculated using the corresponding core volume (Indoria et al., 2020). Gravimetric soil water content was converted to volumetric soil water content using ρ_b values. The soil pH and EC were measured using pH and EC meters, respectively. Soil organic matter (SOM) was measured using the loss-on-ignition method (Kroetsch and Wang, 2008).

The experiments combined two factors. 1) Tillage system: Conventional tillage (CT) by disc plough and spring-tooth harrow; and no-tillage (NT) which were assigned in the main plots. 2) Organic fertilizer type: Cattle manure (CF; 1250 kg·ha^{-1}), chicken manure (CM; 1250 kg·ha^{-1}); and no fertilizer (NF) were assigned in the sub-plots. A randomized complete block design with a split-plot arrangement was used, with three replicates of each treatment, as shown in Fig. 5.

The CT plots at both sites were ploughed to 20 cm soil depth by disc plough. The soil water content was 15–20 %, as measured by weight. The ploughing cut and turned the surface soil layer, which contained plant remnants. It was followed by harrowing with the spring-tooth harrow to smooth the soil surface. The NT plots were cleaned using simple tools such as sickles, which is the customary practice in Iraq, and the soil was left undisturbed with plant residue.

Organic fertilizers (CF or CM) were added by scattering them on the soil surface of the CT and fertilizer plots, then mixing them into the soil to a depth of 20 cm using toothed combs. However, in the NT and fertilizer plots, the CF and CM were added by scattering and were left

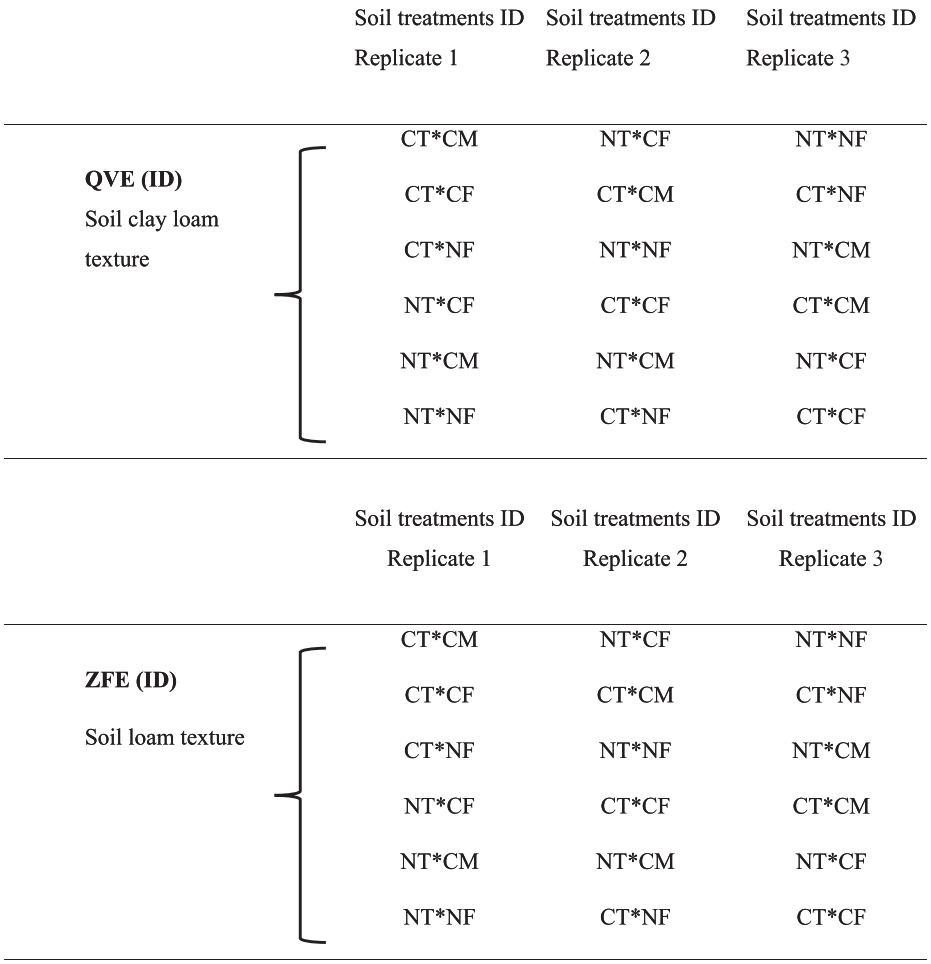

Fig. 5. Schematic diagram of the experimental setup and soil treatments for both experiment sites. QVE: Al Qataniyah village experiment, ZFE: Al-Zafaraniah farm experiment, CT: Conventional tillage, NT: No-tillage, CF: Cattle fertilizer, CM: chicken manure, NF: No fertilizer.

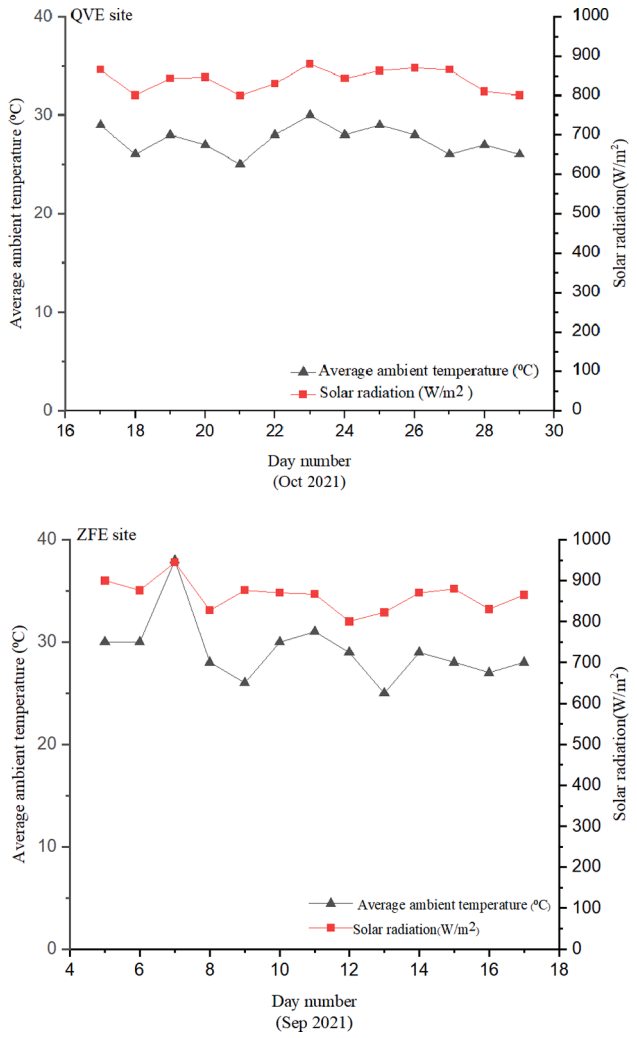

Fig. 6. Average ambient temperature and solar radiation at the Al Qataniyah village experiment (QVE), and Al-Zafaraniah farm experimental (ZFE) sites during the 2 weeks after their preparation.

undisturbed on the soil surface. Both sites were left for two weeks to allow for partial decomposition of the fertilizers. As shown in Fig. 6, the average ambient temperature and solar radiations were 28 °C and 880 $W{\cdot}m^{-2}$, respectively-two weeks after measurements preparation.

2.4. Calculations and statistics

The soil thermal conductivity (λ) is calculated using the following equation (Hillel, 2003).

$$\lambda = \frac{Q^{*}L}{A^{*}\Delta T} \tag{1}$$

where Q (W) is the electrical power consumed by the heater during a unit time, L (m) is the length of the soil column sample, A (m^2) is the cross-sectional area of the soil sample, and ΔT (K) is the temperature difference between the two thermocouples located of the soil sample with time.

Results obtained from measurements with the new HPP according to Eq. (1) were compared to λ estimated from a pedotransfer function (Kersten function). The selected pedotransfer function was used because it produced good results to various textures in Iraqi soils in the medium-textured soil group (Jameel Kareem Al-Lame and NA Al-Saadoon, 2020), and is presented in Eq. (2) (Evett et al., 2012).

$$\lambda = 0.1442(0.9\,log\theta - 0.2)10^{0.01\rho_b} \tag{2}$$

where θ is the soil water content (%), and ρ_b is the soil dry bulk density ($g{\cdot}cm^{-3}$).

The root mean square error (RMSE), mean of absolute error (MAE), and standard deviation of the prediction error (SDPE) were used to compare the performance of the new HPP compared to the pedotransfer function under different agricultural managements, as well as soil depth for the two experimental sites according to the following expressions:

$$RMSE_P\lambda = \sqrt{\frac{\sum_{i=1}^{n}(\lambda_{HPP} - \lambda_{PTF})^2}{n}} \tag{3}$$

$$\mathrm{MAE}\,\lambda = \frac{1}{n}\sum_{i=1}^{n}|\lambda_{HPP} - \lambda_{PTF}| \tag{4}$$

$$SDPE\,\lambda = \sqrt{\frac{1}{n-1}\sum_{i=1}^{n}[(\lambda_{HPP} - \lambda_{PTF}) - MAE]^2} \tag{5}$$

where λ_{HPP} is soil thermal conductivity measured by the new HPP, λ_{PTF} is soil thermal conductivity estimated using the pedotransfer function from Eq. (2), and n corresponds to the total number of measurements.

3. Results and discussion‘

3.1. Soil properties at the experimental sites

As shown in Table 1, both experimental sites had a close the size distribution of silt particles. Soil analysis results show that the θ values for the QVE were 20.7, 24.2, and 28.6 % at 0–5, 5–10, and 10–15 cm soil depths, respectively. In the ZFE, the θ values were 18, 25, and 27 % at 0–5, 5–10, and 10–15 cm soil depths, respectively. These results indicate that θ increases with soil depth due to weather and evaporation from the soil surface. The soil organic matter (SOM) content at all three depths was slightly higher for the QVE than for the ZFE. The highest SOM of 8 % occurred in the QVE at 5–10 cm soil depth, while the lowest occurred in the ZFE and was 7 % at 5–10 cm. Soil ρ_b increased significantly with depth at both sites and was influenced by natural soil compaction and past agri-management practices. Therefore, the highest ρ_b occurred at 10–15 cm depth, with values of 1.42 g cm^{-3} and 1.51 g cm^{-3} for the QVE and ZFE sites respectively. The pH and EC were measured at both sites and values are shown in Table 1. The highest pH value of 7.14 occurred for the QVE at 5–10 cm soil depth, whereas, the lowest value 7.00 for the ZFE at 10–15 cm depths. Thus, soil depths increased led to a significant dicreased in pH values, which explained the raised organic matter of soil in the QVE site compared with ZFE site. EC of soil samples ranged from 1.79 to 1.66 $ds{\cdot}m^{-1}$ at 0–5 cm and 10–15 cm depth, respectively at QVE site, the EC values for the ZFE ranged from 1.76 to 1.62 $ds{\cdot}m^{-1}$.

3.2. Soil λ measurements

Measurements of λ using the HPP and estimates from pedotransfer function are shown in Fig. 7. Measurements show that λ is highly dependenton the tillage practices, fertilizer type, soil depth, and soil texture. Fig. 7 also shows that the average λ for the different soil treatments increased with soil depth according to both methodologies. This is due to the increase in soil water content with depth as λ highly depends on θ.

There were no significant differences in λ related to the site, tillage practices, or measurement method ($p = 0.05$; Fig. 7b-c measured by HPP; Fig. 7d-e measured by Kersten function). The highest average λ measured by the HPP was obtained at the QVE site (clay loam), NT treatment showed the highest average λ with a value of 0.85 $W{\cdot}m^{-1}{\cdot}K^{-1}$ at 10–15 cm depth (Fig. 7c), whereas the CT treatment showed a lower λ of 0.70 $W{\cdot}m^{-1}{\cdot}K^{-1}$ at 0–5 cm soil depth (Fig. 7a). At the ZFE site (loam)

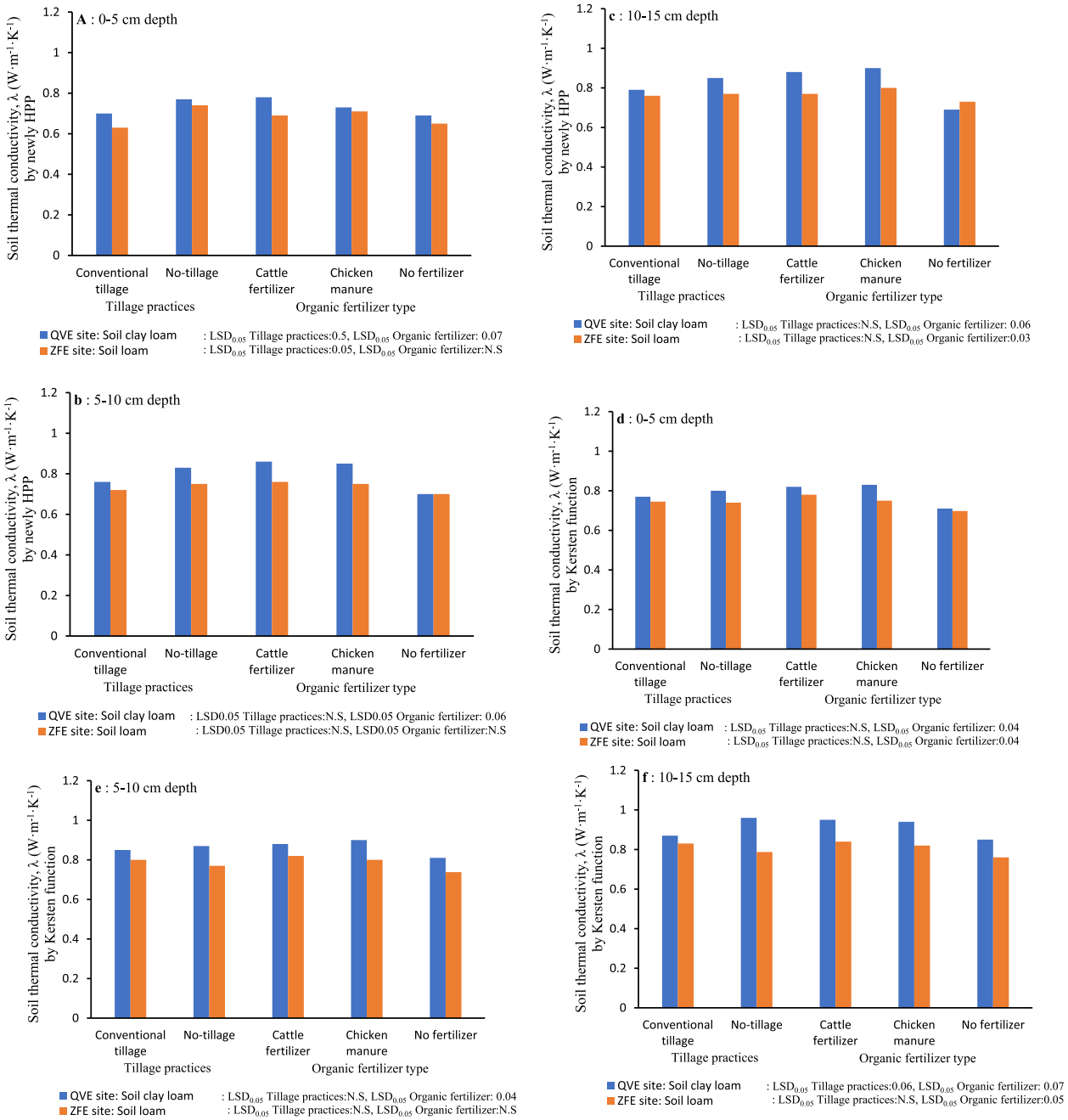

Fig. 7. Average soil thermal conductivity, λ ($W{\cdot}m^{-1}{\cdot}K^{-1}$), measured by HPP and Kersten function at the two experimental sites with different tillage practices, fertilizer types, and soil samples were taken at three distinct depths: 0–5 cm, 5–10 cm, and 10–15 cm soil depths, average +/- standard deviation error 0.01.

the NT treatment also showed a higher λ with a value of 0.77 $W{\cdot}m^{-1}{\cdot}K^{-1}$ at 10–15 cm depth, while for the CT treatment it decreases to 0.63 $W{\cdot}m^{-1}{\cdot}K^{-1}$ at 0–5 cm depth.

Estimates values of λ using the pedotransfer function were also determined for the two sites. At the QVE site, the NT practice showed the highest average λ with a value of 0.96 $W{\cdot}m^{-1}{\cdot}K^{-1}$ at 10–15 cm depth (Fig. 7f), while CT showed a lower value of 0.77 $W{\cdot}m^{-1}{\cdot}K^{-1}$ at 0–5 cm depth (Fig. 7d). The higher λ in for NT is attributed to the increases in soil water content and bulk density. Furthermore, NT has greater energy exchange than the CT practices because of the increased heat transfer, which is dependent on bulk density and soil water content (Dai et al., 2021).

Fig. 7, shows that organic fertilizer had a significant influence on λ for most soil treatments at both sites due to the contrasting thermal behaviour of the organic matter compared to the mineral soil fraction. The λ measured by the HPP at the QVE site (clay loam) had the highest average λ (0.90 $W{\cdot}m^{-1}{\cdot}K^{-1}$ in the CM treatment at 10–15 cm soil depth), while the lowest average λ was 0.68 $W{\cdot}m^{-1}{\cdot}K^{-1}$ measured in the NF treatment at 10–15 cm soil depth.

Measurements of λ by the HPP at the ZFE site (loam) also showed that the CM treatment had the highest average λ with a value of 0.80 $W{\cdot}m^{-1}{\cdot}K^{-1}$ at 10–15 cm depth, while the lowest average λ was 0.65 $W{\cdot}m^{-1}{\cdot}K^{-1}$ for the NF treatment at 0–5 cm depth. A possible explanation may be that the CM treatment increases θ by increasing SOM. SOM increases the activity of microorganisms in the soil because it provides an additional source of energy and increases the soil waterholding capacity. The products of the microorganism activities help bound soil particles, reduce soil bulk density, and increase the soil water holding capacity. These results agree with the findings of (Agbede, 2021; He et al., 2022; Rombolà et al., 2022). Results show that measurements of λ by the HPP

produced similar or even smaller values than those estimated by the pedotransfer function.

3.3. Comparison of λ measured by the HPP and estimated from PTF

Results of the comparison between λ measured by the HPP and the corresponding estimate from the pedotransfer function, use the coefficient of determination (R^2), the standard deviation (σ), the standard error of the mean (SEM), the coefficient of variation (CV), the root mean square error (RMSE), the mean absolute error (MAE), and the regression equation as presented in Fig. 8. It shows a strong relationship between both methods at both experimental sites. At the 05– cm depth, linear regression of HPP against pedotransfer function provided an R^2 of 0.92, RMSE of 0.092 $W{\cdot}m^{-1}{\cdot}K^{-1}$, and MAE of 0,080 $W{\cdot}m^{-1}{\cdot}K^{-1}$. (Fig. 8a). At the 5–10 cm depth, the linear regression analysis provided a slightly lower R^2 of 0.88, a slightly higher RMSE of 0.090 $W{\cdot}m^{-1}{\cdot}K^{-1}$, and MAE of 0.076 $W{\cdot}m^{-1}{\cdot}K^{-1}$; while at 10–15 cm depth, the R^2, RMSE, and MAE were similar or even smaller than at 5–10 cm depth. Lower RMSE values indicate better agreement, which can be achieved in the field using the HPP under different field conditions. Consequently, in the agreement of the λ values as measured by the new HPP or estimated from the pedotransfer function increased with soil water content and bulk density.

In addition, Fig. 8 shows that the CV of λ measured by the HPP is lower (8.53 %) than that obtained from the pedotransfer function (11.7 %) at 0–5 cm depth. At the 5–10 cm depth, measurements by the HPP have a higher CV of 10.2 %, compared with the estimated from the pedotransfer function with a value of 7.84 %.

Dispersion indexes σ and SEM of the λ measurements by the HPP and estimated from the pedotransfer function were also calculated. At 0–5 cm depth, σ and SEM, as measured from the HPP, were 0.061 $W{\cdot}m^{-1}{\cdot}K^{-1}$ and 0.010 $W{\cdot}m^{-1}{\cdot}K^{-1}$, respectively, lower compared to those obtained from the pedotransfer function (0.085 $W{\cdot}m^{-1}{\cdot}K^{-1}$ and 0.014 $W{\cdot}m^{-1}{\cdot}K^{-1}$, respectively). However, at 5–10 cm depth, σ and SEM form as measured by the HPP (0.077 $W{\cdot}m^{-1}{\cdot}K^{-1}$ and 0.0129 $W{\cdot}m^{-1}{\cdot}K^{-1}$ respectively) were slightly higher than those of estimated from the pedotransfer function (0.066 $W{\cdot}m^{-1}{\cdot}K^{-1}$ and 0.011 $W{\cdot}m^{-1}{\cdot}K^{-1}$ respectively).

The correlation between measured λ by the HPP and estimated from the pedotransfer function is presented in Fig. 8 for the three depths considering the different soil treatments. Results show that uncertainty

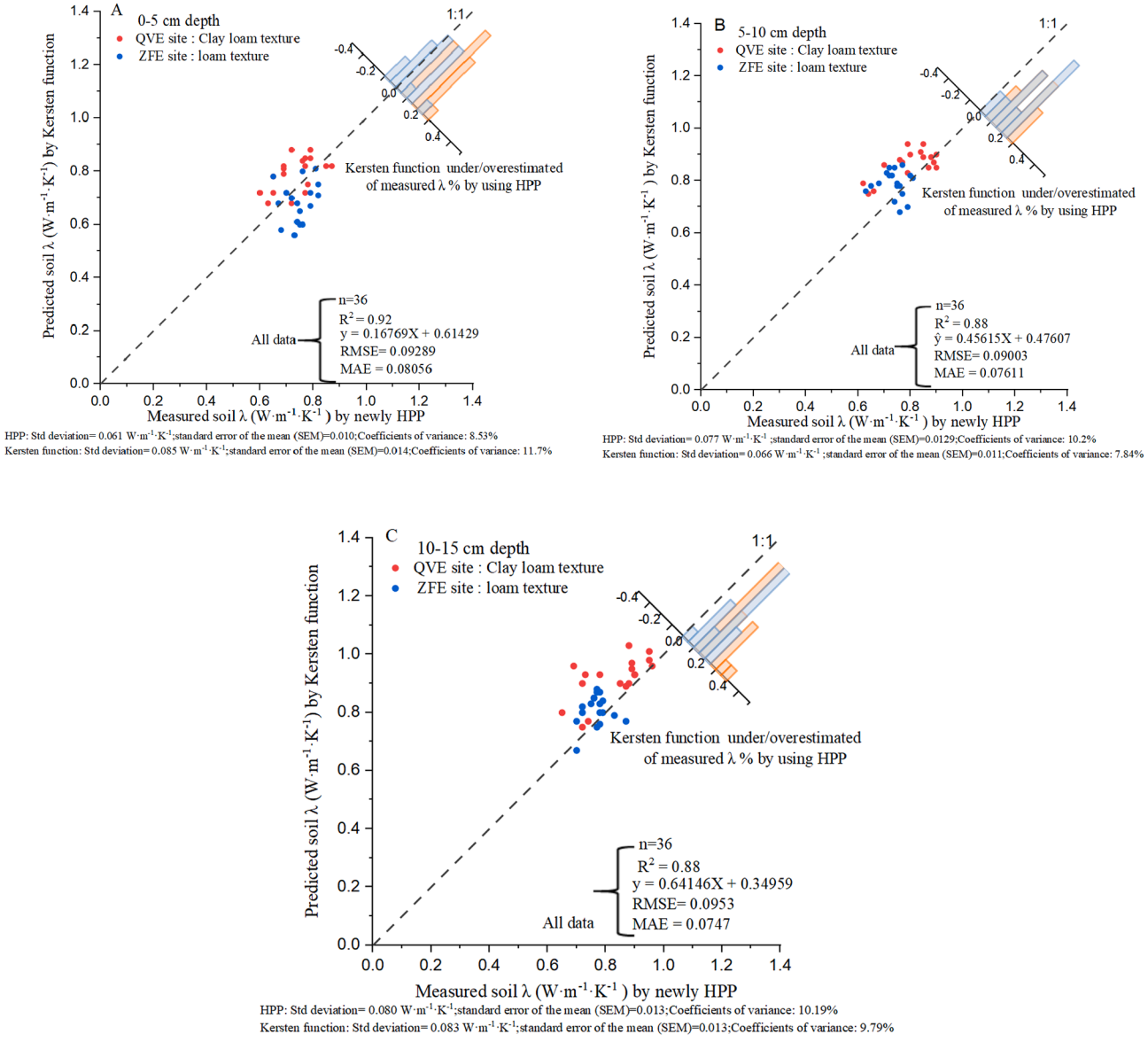

Fig. 8. Soil thermal conductivity, λ, measured by the HPP and estimated from the Kersten function for the two experimental sites at three depths. The RMSE, MAE, and regression equation are shown for three depths. The histogram of measurement from the HPP is shown in the corner of the scatter graph.

in λ measured by the HPP is lower than estimated from the pedotransfer function, but measurements were influenced by the type of soil treatment, soil water content, bulk density, and soil texture.

The pedotransfer function under/overestimated λ was measured using the HPP in all soil treatments and depths (Fig. 8), with ranges of −0.17 to 0.16 %, −0.09 to 0.16 %, and − 0.04 to 0.27 %, 0–5, 5–10, and 10–15 cm soil depths, respectively (Fig. 8 inset). A probable explanation is that these differences were due to spatial asymmetry at the study sites, resulting in different θ in the measured λ, measurement times, and soil disturbance at the treatment plots. Furthermore, soil porosity also influences λ (Usowicz et al., 2006).

In addition to the MBE of the λ measurements by the HPP, Table 2 also shows the SDPE and the CV. Results indicate that λ from HPP has a high degree of precision in measuring λ based on the low MPE values for most soil treatments. The precision of λ measurements using the HPP is affected by soil texture, soil water content, bulk density, and agricultural management practice (Sahoo et al., 2019).

Measurements of λ with the HPP showed small MPE values of 0.02 $W{\cdot}m^{-1}{\cdot}K^{-1}$ for soil treatments (interaction of tillage management and fertilizer type; NT*CM at 0–5 cm depth; CT*NF and NT*CF at 5–10 depth; NT*NF at 10–15 cm depth) at the QVE site (clay loam soil), while at ZFE site the MPE values were 0.01 $W{\cdot}m^{-1}{\cdot}K^{-1}$ for some of the soil treatments (CT*CM, CT*CF, and CT*NF at 10–15 cm depth (Table 2)). The SDPE for both sites and at all depths was rather similar and low for all soil treatments. The CV for the λ measurements by the HPP was higher than those from the pedotransfer function at 5–10 cm and 10–15 cm depth. A possible explanation is the changes in ρ_b and θ between soil treatments, which were measured in-situ at both sites. Further changes in SOM are also influenced by the tillage practice, fertilizer type, and soil depth. The ρ_b and θ were measured for calculating λ by the pedotransfer function developed by Kersten (1949) at 0–5, 5–10, and 10–15 cm depths, under the two tillage practices and three fertilizer types. Both experimental sites are shown in Fig. 9. It can be seen that the soil ρ_b at both sites increased with depth. The NT treatment exhibited higher ρ_b values at both sites and all depths (Fig. 9a) because of the past management practices used and the presence of organic matter (Jahanger, 2021). Results in Fig. 9 show that θ increased with conventional tillage treatment and soil depth at both sites. For example, at the QVE site, CT showed the highest average θ values of 0.29, 0.33, and 0.44 % at the 0–5, 5–10, and 10–15 cm depth, respectively, while the NT treatment showed lower average θ values of 0.22, 0.28, and 0.34 %, respectively (Fig. 9c). The ZFE site also showed for CT a higher average θ with depth. Possibly this is due to CT enhancing the water-holding capacity of the soil, leading to an increase in θ (Zhao et al., 2019).

Fig. 9 also reveals that there were slower decreases in ρ_b with depth in treatments CF and CM compared to NF. For example, at the QVE site, lower average ρ_b values of 1.25 and 1.33 $g{\cdot}cm^{-3}$ were measured in treatments CF and CM, and a higher average of 1.33 $g{\cdot}cm^{-3}$ in NF treatment at 0–5 cm depth. The results also show that increases in soil ρ_b values with depth were greater for most organic fertilizer treatments due to increases in soil structural stability. Fig. 9 shows that organic fertilizer had a significant impact on the soil θ at the QVE site, which exhibited a higher average θ (0.27 %) than those obtained for the CF and CM treatments at 0–5 depth. The θ values increased with depth in all treatments at both sites. These results are explained by the local weather conditions at the surface at the time where measurements were taken.

3.4. ΔT of soils during HPP testing under different soil treatments

Fig. 10 provides an overview of the difference in soil temperature (ΔT) with heating time for the different treatments, depths, and sites. Fisher's least significant difference (LSD) procedure is used to compare soil treatments on average soil temperature (ΔT). The LSD analysis revealed no significant differences in ΔT with tillage practices at 5–10, 10–15 cm depths at both sites. However, at the QVE site, the average ΔT at 0–5, 5–10, and 10–15 cm depth results higher for CT with values of 18.4, 16.5, and 15.5 °C compared to no-tillage NT with average values of 16.1, 14.7, and 14.8 °C for the three depths considered, respectively. Similarly, for soil treatments at the ZFE site, the average ΔT at the 0–5 cm depth was slightly higher than at other depths. In both tillage practices (CT: 19.8 °C at 0–5 cm depth, 17.4 °C, and 16.5 °C at 5–10, 10–15 cm depths, respectively; NT: 16.9 °C at 0–5 cm soil depth, 16.5, 16.3 °C at 5–10, 10–15 cm depth, respectively). This result may be explained by a decrease in soil ρ_b and increase in soil water content due to tillage practices, which lead to an increase in temperature flow (Dai et al., 2021), or due to the effect of soil type with depth, or SOM (Jahanger, 2021).

Fertilizer treatments significantly increase ΔT recorded at all depths ($P < 0.05$; Fig. 10). It is to be noted that NT showed a higher average ΔT of 18.5, 18, and 17.6 °C with increasing depth (0–5, 5–10, and 10–15 cm depths, respectively) at both sites compared to the CF and CM treatments. This might be related to fertilizer being able to increase ΔT due to an increased SMO and soil structural stability for NF practices.

3.5. Estimated cost and indications for the new HPP

The HPP total cost is estimated in Table 3. The cost of a complete unit, including ECS and MC, is approximately US$83. The housings of

Table 2
Mean bias error and standard deviation of the prediction error of measured soil thermal conductivity, λ by the HPP for the two experimental sites at three depths with different management treatments.

Site	Treatments	Depth (cm)								
		0–5			5–10			10–15		
		[1] MBE $W{\cdot}m^{-1}{\cdot}K^{-1}$	[2] SDPE $W{\cdot}m^{-1}{\cdot}K^{-1}$	CV %	MBE $W{\cdot}m^{-1}{\cdot}K^{-1}$	SDPE $W{\cdot}m^{-1}{\cdot}K^{-1}$	CV %	MBE $W{\cdot}m^{-1}{\cdot}K^{-1}$	SDPE $W{\cdot}m^{-1}{\cdot}K^{-1}$	CV %
QVE	CT*CM	0.05	0.037	6.2	0.07	0.044	6.5	0.07	0.049	7.0
	CT*CF	0.07	0.049	8.6	0.06	0.056	6.9	0.03	0.020	2.8
	CT*NF	0.03	0.020	4.0	0.02	0.016	3.1	0.05	0.038	6.7
	NT*CF	0.05	0.033	4.9	0.02	0.016	2.2	0.05	0.033	4.5
	NT*CM	0.02	0.012	1.9	0.03	0.020	2.8	0.04	0.028	3.7
	NT*NF	0.04	0.032	5.5	0.05	0.037	6.1	0.02	0.016	2.9
ZFE	CT*CM	0.04	0.030	6.0	0.04	0.032	5.3	0.01	0.008	1.2
	CT*CF	0.04	0.029	5.2	0.02	0.016	2.6	0.01	0.004	0.7
	CT*NF	0.02	0.016	3.7	0.03	0.020	3.8	0.01	0.009	1.6
	NT*CF	0.05	0.036	5.9	0.05	0.038	6.2	0.02	0.012	1.9
	NT*CM	0.07	0.054	9.0	0.03	0.026	4.3	0.06	0.045	6.7
	NT*NF	0.05	0.041	6.9	0.03	0.020	3.2	0.05	0.035	5.8

[1]Mean bias error; [2] Standard deviation of the prediction error
*Combination of tillage management and fertilizer

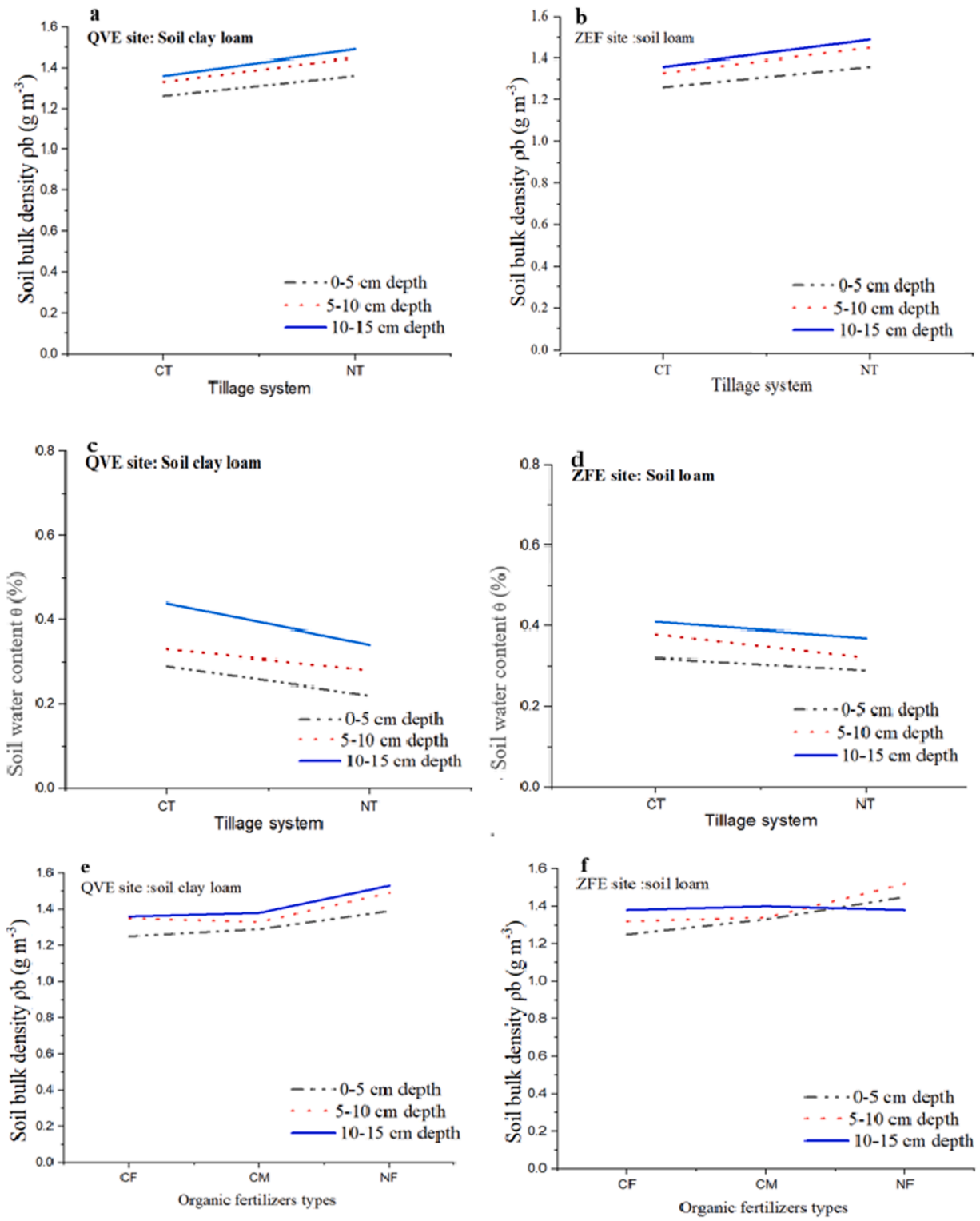

Fig. 9. Soil bulk density ρb ($g{\cdot}cm^{-3}$) and soil water content θ (%) measured at the two experimental sites and three depths with different tillage practices and fertilizer types (average +/- 0.01 standard deviation).

both the ECS and MC units were made of 1 cm-thick stainless steel, which has an approximate cost of US$1.71. The penetration probe with two thermocouple sensors cost US$10. The electronic components (2 Arduino, LCD, Acs 712 sensor, 315 MHz RF Transmitter, Receiver Module, and Bluetooth module (HC-05)) cost US$47.8. Hence, the novel HPP is low-cost and highly energy efficient compared to a transient line source (TLS-100), with a cost almost two orders of magnitude higher. All sensors and electronic parts used in the new HPP are available at http://www.uruktech.com.

The new HPP design can be used in the laboratory or on-site according to the needs. It is of special interest in soil physics and particularly experiments or measurements related to the thermal properties of

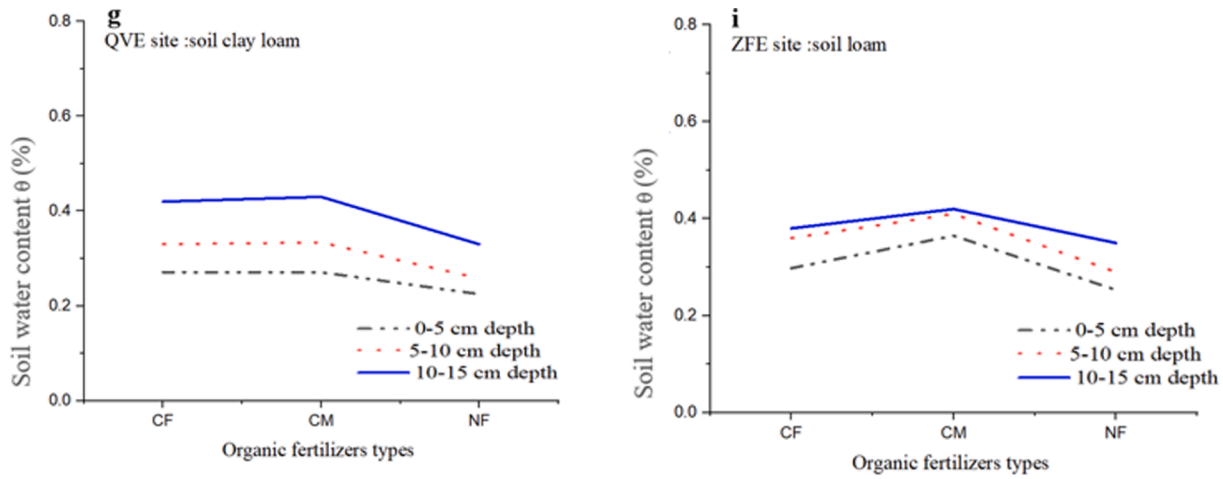

Fig. 9. (*continued*).

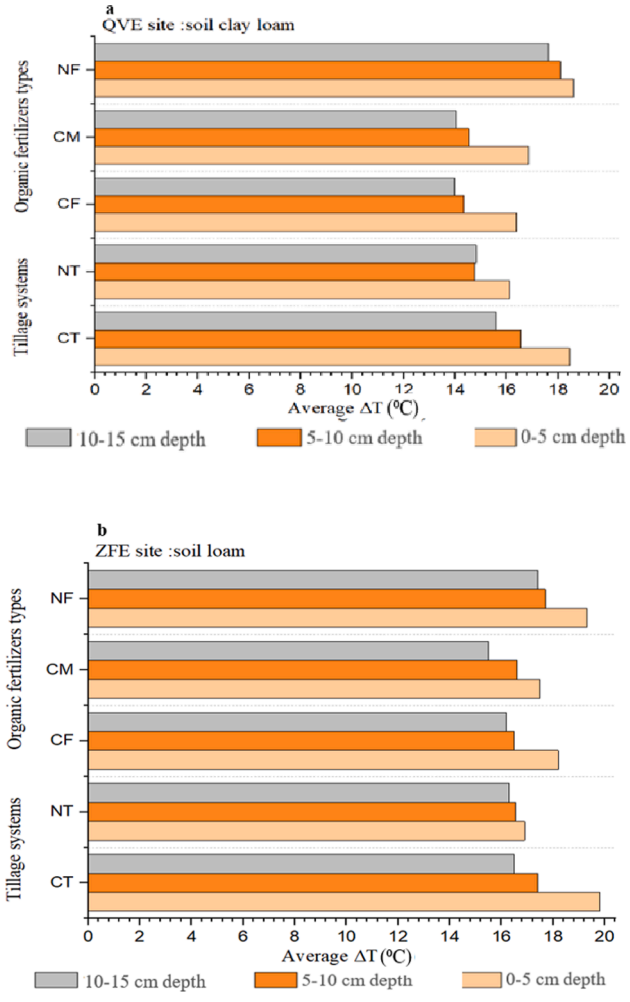

Fig. 10. Soil temperature difference (ΔT) at two points installed in the penetration probe after heating up (based on preset actions in the newly HPP). Notes: the least significant difference (LSD) values between treatments are shown in the analysis as follows: For the QVE site: Tillage practice at 0–5 cm depth: 1.31; Tillage practice at 5–10 cm depth: N.S; Tillage practice at 10–15 cm depth: N.S, for fertilizer type at 0–5 cm depth: 1.90; fertilizer type at 5–10 cm depth: 1.73; fertilizers type at 10–15 cm depth: 1.07. For the ZFE site: Tillage practice at 0–5 cm depth: 1.43; Tillage practice at 5–10 cm depth: N.S; Tillage practice at 10–15 cm depth: N.S, for fertilizer type at 0–5 cm depth: N.S; fertilizer type at 5–10 cm depth: 1.29; fertilizer type at 10–15 cm depth: 0.60).

Table 3
Cost estimation of the HPP.

Item	Quantity	Cost $
Liquid Crystal Display	1	2.91
Arduino	2	30
Acc	1	6.2
315Mhz RF Transmitter and Receiver Module	1	1.7
Bluetooth module HC-05	1	7
Thermocouples sensor with MAX6675 thermocouple operation amplifier	2	24.8
5 v relay module	1	2.0
Electric Heater 12v	1	7.0
Thermal insulation	–	0.5
Insulation pipe	–	0.5
Cylindrical plate	0	0.5
–	Total	83.11

soils. The new HPP can measure the thermal conductivity of all types of fine and cohesive soils. However, it is not the preferred choice for use with sandy and gravelly soils because of the difficulty in obtaining a sufficient soil volume.Although the HPP can be used within a broad range of soil water content, the HPP was tested measuring the soil thermal conductivity within a limited soil water content range (18–29 %), potential measuerment errors out of this range would be evaluated in a future work. Furthermore, the new HPP is distinguished by its ability to be used in the field while powered by solar cells. All components are easily available and it is reasonably simply to build.

4. Conclusions

A novel heat-pulse probe (HPP) is designed to estimate soil thermal conductivity (λ). It can measure λ with higher reliability than estimates made using pedotransfer functions (PTFs; Kersten function). The results of this study show that the tillage practice, fertilizer type, soil water content, bulk density, and soil texture significantly influence λ. A no-tillage practice has greater energy exchange than a conventional tillage practice due to increased heat transfer, which is dependent on the particle size distributions of the soil layers and soil depth. The comparison of λ measurements using the HPP versus estimates from the pedotransfer function shows that the HPP has a high degree of precision, exhibiting low mean bias errors for the majority of soil treatments. The mean bias error and standard deviation of the prediction error and effect by soil texture, soil water content, bulk density, and agricultural practices. Underestimates and overestimates in λ measured by the new HPP were quantified. The new HPP was set up using commercially available materials, is low-cost, and easy to maintain and operate. As there are no

limiting tools, it can be easily manufactured. Further research should investigate the performance of the HPP in measuring soil thermal conductivity for additional soil types and conditions.

CRediT authorship contribution statement

Ahmed Abed Gatea Al-Shammary: Conceptualization, Methodology, Software, Data curation, Writing – original draft, Writing – review & editing. **Andrés Caballero-Calvo:** Formal analysis, Resources, Writing – original draft, Writing – review & editing. **Hussein Abbas Jebur:** Visualization, Investigation, Software, Validation. **Mohanad Ismael Khalbas:** Methodology, Formal analysis, Validation. **Jesús Fernández-Gálvez:** Conceptualization, Methodology, Validation, Writing – review & editing, Supervision.

Declaration of Competing Interest

The authors declare that they have no known competing financial interests or personal relationships that could have appeared to influence the work reported in this paper.

Data availability

Data will be made available on request.

References

Agbede, T.M., 2021. Effect of tillage, biochar, poultry manure and NPK 15–15-15 fertilizer, and their mixture on soil properties, growth and carrot (Daucus carota L.) yield under tropical conditions. Heliyon 7, e07391.

Al-Maliky, S.J.B., 2011. Investigation of the readiness of ground soils for the installation of ground heat exchange systems in Baghdad city. J. Geogr. Geol. 3, 200.

ASTM, 2010. Standard test methods for laboratory determination of water (moisture) content of soil and rock by mass. D2216-10). ASTM International, West Conshohocken, PA. doi 10.

Bristow, K.L., 1998. Measurement of thermal properties and water content of unsaturated sandy soil using dual-probe heat-pulse probes. Agric. For. Meteorol. 89 (2), 75–84.

Chen, Z.X., Guo, X.X., Shao, L.T., Li, S.Q., 2020. On determination method of thermal conductivity of soil solid material. Soils Found. 60 (1), 218–228.

Dai, Z., Hu, J., Fan, J., Fu, W., Wang, H., Hao, M., 2021. No-tillage with mulching improves maize yield in dryland farming through regulating soil temperature, water and nitrate-N. Agric. Ecosyst. Environ. 309, 107288.

Dong, Y., Lu, N., Wayllace, A., Smits, K., 2014. Measurement of thermal conductivity function of unsaturated soil using a transient water release and imbibition method. Geotech. Test. J 37, 980–990.

Du, Y., Li, R., Wu, T., Yang, C., Zhao, L., Hu, G., Xiao, Y., Yang, S., Ni, J., Ma, J., Shi, J., Qiao, Y., 2022. A new model for predicting soil thermal conductivity for dry soils. Int. J. Thermal Sci. 176, 107487.

Evett, S.R., Agam, N., Kustas, W.P., Colaizzi, P.D., Schwartz, R.C., 2012. Soil profile method for soil thermal diffusivity, conductivity and heat flux: Comparison to soil heat flux plates. Adv. Water Resour. 50, 41–54.

He, H., Dyck, M.F., Horton, R., Li, M., Jin, H., Si, B., 2018a. Distributed temperature sensing for soil physical measurements and its similarity to heat pulse method. Adv. Agron. 148, 173–230.

He, H., Dyck, M.F., Horton, R., Ren, T., Bristow, K.L., Lv, J., Si, B., 2018b. Development and application of the heat pulse method for soil physical measurements. Rev. Geophys. 56 (4), 567–620.

He, H., Dyck, M., Lv, J., 2020a. The heat pulse method for soil physical measurements: a bibliometric analysis. Appl. Sci. 10, 6171.

He, R., Jin, H., Jia, N., Wang, H., Jin, X., Li, X., 2022. Thermal conductivity contrast effect of organic soils and its environmental implications. Cold Regions Sci. Technol. 196, 103485.

He, H., Noborio, K., Johansen, Ø., Dyck, M.F., Lv, J., 2020b. Normalized concept for modelling effective soil thermal conductivity from dryness to saturation. Eur. J. Soil Sci. 71, 27–43.

Hillel, D., 2003. Introduction to environmental soil physics. Elsevier.

Huluka, G., Miller, R., 2014. Particle size determination by hydrometer method. Southern Cooperative Ser. Bull. 419, 180–184.

Indoria, A.K., Sharma, K.L., Reddy, K.S., 2020. Chapter 18 - Hydraulic properties of soil under warming climate. In: Prasad, M.N.V., Pietrzykowski, M. (Eds.), Climate Change and Soil Interactions. Elsevier, pp. 473–508.

Jahanger, Z.K., 2021. Evaluation of the thermal conductivity of middle part of Iraqi soil. Mater. Today:. Proc. 42, 2431–2435.

Jameel Kareem Al-Lame, A., NA Al-Saadoon, J., 2020. Study The thermal properties of the soil under systems irrigation and mulching different. Al-Qadisiyah J. Agric. Sci. 10, 415–425.

Kersten, M.S., 1949. Thermal properties of soils.

Knight, J.H., Kluitenberg, G.J., Kamai, T., Hopmans, J.W., 2012. Semianalytical solution for dual-probe heat-pulse applications that accounts for probe radius and heat capacity. Vadose Zone J. 11 (2).

Kojima, Y., Kawashima, T., Noborio, K., Kamiya, K., Horton, R., 2021. A dual-probe heat pulse-based sensor that simultaneously determines soil thermal properties, soil water content and soil water matric potential. Comput. Electron. Agric. 188, 106331.

Kroetsch, D., Wang, C., 2008. Particle size distribution. Soil sampling and methods of analysis 2, 713-725.

Liu, G., Lu, Y., Wen, M., Ren, T., Horton, R., 2020. Advances in the heat-pulse technique: Improvements in measuring soil thermal properties. Soil Sci. Soc. Am. J. 84, 1361–1370.

Lu, S., Ren, T., Horton, R., 2020. Estimating the components of apparent thermal conductivity of soils at various water contents and temperatures. Geoderma 376, 114530.

Mahdavi, S.M., Neyshabouri, M.R., Fujimaki, H., 2016. Assessment of some soil thermal conductivity models via variations in temperature and bulk density at low moisture range. Eurasian Soil Sci. 49, 915–925.

Maivald, P., Sridar, S., Xiong, W., 2022. Thermal conductivity determination of Ga-In alloys for thermal interface materials design. Thermo 2, 1–13.

Mirzaei, M., Anari, M.G., Razavy-Toosi, E., Zaman, M., Saronjic, N., Zamir, S.M., Caballero-Calvo, A., 2022. Crop residues in corn-wheat rotation in a semi-arid region increase CO_2 efflux under conventional tillage but not in a no-tillage system. Pedobiologia. https://doi.org/10.1016/j.pedobi.2022.150819.

Morris, N.L., Miller, P.C.H., Orson, J.H., Froud-Williams, R.J., 2010. The adoption of non-inversion tillage systems in the United Kingdom and the agronomic impact on soil, crops and the environment—A review. Soil Tillage Res. 108, 1–15.

Muhammad, G., Marri, A., Shar, A.M., 2018. Development of experimental setup for measuring thermal conductivity characteristics of soil. Mehran Univ. Res. J. Eng. Technol. 37, 559–568.

Nikoosokhan, S., Nowamooz, H., Chazallon, C., 2016. Effect of dry density, soil texture and time-spatial variable water content on the soil thermal conductivity. Geomech. Geoeng. 11, 149–158.

Rombolà, A.G., Torri, C., Vassura, I., Venturini, E., Reggiani, R., Fabbri, D., 2022. Effect of biochar amendment on organic matter and dissolved organic matter composition of agricultural soils from a two-year field experiment. Sci. Total Environ. 812, 151422.

Romio, L.C., Roberti, D.R., Buligon, L., Zimmer, T., Degrazia, G.A., 2019. A numerical model to estimate the soil thermal conductivity using field experimental data. Appl. Sci. 9, 4799.

Różański, A., 2022. Relating thermal conductivity of soil skeleton with soil texture by the concept of "local thermal conductivity fluctuation". J. Rock Mech. Geotech. Eng. 14, 262–271.

Sahoo, A.K., Mallik, S., Pradhan, C., Mishra, B.S.P., Barik, R.K., Das, H., 2019. Intelligence-Based Health Recommendation System Using Big Data Analytics. In: Dey, N., Das, H., Naik, B., Behera, H.S. (Eds.), Big Data Analytics for Intelligent Healthcare Management. Academic Press, pp. 227–246. Chapter 9.

Sandholt, I., Rasmussen, K., Andersen, J., 2002. A simple interpretation of the surface temperature/vegetation index space for assessment of surface moisture status. Remote Sens. Environ. 79, 213–224.

Schjønning, P., 2021. Thermal conductivity of undisturbed soil – Measurements and predictions. Geoderma 402, 115188.

Shiozawa, S., Campbell, G.S., 1990. Soil thermal conductivity. Remote Sens. Rev. 5, 301–310.

Sparks, D.L., Page, A.L., Helmke, P.A., Loeppert, R.H., 2020. Methods of soil analysis, part 3: Chemical methods. John Wiley & Sons.

Staff, S.S., 2014. Keys to soil taxonomy. United States Department of Agriculture, Washington, DC, USA.

Taghizadeh-Toosi, A., Elsgaard, L., Clough, T.J., Labouriau, R., Ernstsen, V., Petersen, S. O., 2019. Regulation of N_2O emissions from acid organic soil drained for agriculture. Biogeosciences 16, 4555–4575.

Tarnawski, V.R., Coppa, P., Leong, W.H., McCombie, M., Bovesecchi, G., 2020. On modelling the thermal conductivity of soils using normalized-multi-variable pedotransfer functions. Int. J. Therm. Sci. 156, 106493.

Usowicz, B., Lipiec, J., Ferrero, A., 2006. Prediction of soil thermal conductivity based on penetration resistance and water content or air-filled porosity. Int. J. Heat Mass Transf. 49, 5010–5017.

Walczak, R., Usowicz, B., 1994. Variability of moisture, temperature and thermal properties in bare soil and in crop field. Int. Agrophysics 8, 161–168.

Wang, J., He, D., Dyck, M., He, H., 2020. Theory and solutions of heat pulse method for determining soil thermal properties. In: IOP Conference Series: Earth and Environmental Science. IOP Publishing, p. 052039.

Wang, M., Li, X., Xu, X., 2021. An implicit Heat-Pulse-Probe method for measuring the soil ice content. Appl. Therm. Eng. 196, 117186.

Zhang, X., Heitman, J., Horton, R., Ren, T., 2014. Measuring near-surface soil thermal properties with the heat-pulse method: correction of ambient temperature and soil-air interface effects. Soil Sci. Soc. Am. J. 78 (5), 1575–1583.

Zhao, X., Zhou, G., Jiang, X., 2019. Measurement of thermal conductivity for frozen soil at temperatures close to 0 °C. Measurement 140, 504–510.

Zhaoxiang, T., Jingsen, Z., 1983. The thermal conductivity of thawed and frozen soils with high water (ice) content. J. Glaciol. Geocryol. 5, 75–80.

Zhou, L., Dickinson, R.E., Tian, Y., Vose, R.S., Dai, Y., 2007. Impact of vegetation removal and soil aridation on diurnal temperature range in a semiarid region: application to the Sahel. Proc. Natl. Acad. Sci. 104, 17937–17942.